Journal of Energy Storage 14 (2017) 94–105

Contents lists available at ScienceDirect

Journal of Energy Storage

journal homepage: www.elsevier.com/locate/est

Simulation of thin-film battery response to periodic loading by a transition matrix approximation using boundary and nonlinearity error analysis

Kendall Teichert*, Kenn Oldham

Department of Mechanical Engineering, University of Michigan, 2350 Hayward, Ann Arbor, MI 48109, United States

ARTICLE INFO

Article history:
Received 11 July 2017
Received in revised form 22 August 2017
Accepted 25 September 2017
Available online 17 October 2017

Keyword:
Battery modeling
Multiple timescales
Microelectromechanical systems (MEMS)

ABSTRACT

Simulating repeating loading events on dynamic systems can be challenging when large timescale disparities exist coupled with aperiodic effects. Batteries driving switched/pulsed loads represent one such situation. Large timescale disparity can be experienced by solid-state batteries driving switching microactuators or microelectronics, due to extremely short transient response times of microscale systems relative to some of the battery's own dynamics. Projecting state changes over a long series of fast-timescale loading events using a transition matrix approach was shown previously to significantly reduce numerical expense of simulation compared to full modeling. Here we develop an approach for further accelerated simulation of a battery driving a microelectromechanical system (MEMS) actuator that quantifies errors and addresses overhead expenses in projecting battery states across multiple fast events. This is done with a definition of system states that allows efficient transition matrix generation, and an analysis of key errors associated with projection. This error analysis enables targeted modification to the transition matrix during projection. A case study explores these modeling approaches in a capacitively loaded, battery usage scenario of a piezoelectrically-driven microrobot where the proposed improvements reduce the numerical cost (function calls) by over 44x from the prior approach. Conditions for further simplified modeling are discussed.

1. Introduction

Thin-film solid-state batteries provide a convenient power source for many small engineered systems, particularly micro-systems based on integrated circuit and micro-electromechanical system (MEMS) technologies. In many such systems, battery loading occurs as repeated short-duration transient events, such as to drive microactuators or switching electronics in periodic operation. Individual loading events may occur over time periods of just a few microseconds, given the high bandwidths of associated electrical or electromechanical components, while complete battery discharge may occur over several hours. This vast disparity in timescales can make high-fidelity simulation of battery behavior based on physics-based partial differential equation models, very challenging. Nonetheless, such simulation can be beneficial for understanding influences of system-level design choices (i.e. loading frequency and component sizes) on anticipated battery performance or assessing the accuracy of simplified reduced-order or equivalent circuit battery models. This paper thus proposes a strategy for efficiently simulating repeated transient loading effects on a solid-state battery model using a numerically-identified state-transition matrix approach, and illustrates how error analysis of the numerical method can be used to further improve simulation efficiency and/or accuracy.

In general, modeling of power/battery systems can be an important tool for improving design and control, and has been performed in a variety of ways including electrochemical [1–3] and equivalent circuit modeling [4,5]. Different approaches for model reduction have also been attempted to make the system easier to handle. For example, Santhanagopalan et al. [6] compares model reduction strategies for lithium-ion batteries with porous electrodes, for full discharge cycling; Kim and Qiao [7] present a hybrid model that combines simplicity with nonlinear effects with demonstration on a limited number of pulses during discharge;

* Corresponding author. Present address: One University Ave, Trine University, 251 Fawick, Angola, IN 46703, United States.
E-mail address: kbt@umich.edu (K. Teichert).

https://doi.org/10.1016/j.est.2017.09.014
2352-152X/

Nomenclature

Symbol	and description
$\mathbb{Y}$	Normalized lithium concentration, subscript denotes positive electrode (+) or electrolyte (e)
$\mathbb{T}$	Normalized time
$\mathbb{X}$	Normalized spatial location in positive electrode
$\mathbb{D}$	Normalized diffusion coefficient
$\mathbb{I}$	Normalized current
$\mathbb{V}$	Normalized voltage, subscripts denote various locations in the battery
α_a	Anodic charge transfer coefficient subscripts denote positive or negative electrode
$\mathbb{U}$	Normalized open circuit potential
$\mathbf{A}, \mathbf{B}$	Finite difference matrices
$\mathbf{r}$	Finite difference vector containing boundary condition information
p, r, q, s, C	Variables used for finite difference matrix formulation
h	Finite difference element length
τ	Finite difference time step length
$\mathbf{\Phi}$	Transition matrix
$\mathbf{B}^*, \mathbf{r}^*$	Modified matrix/vector accounting for boundary concentrations
$\mathbf{E}$	Error

and Afshar et al. [8] uses a reduction method to address the boundary conditions transforming them to differential equations through linearization.

In microscale applications, it is also important to understand the usage of battery capacity due to the limited payload and footprint available. The effects of intermittent loading on different types of batteries have been discussed in the literature with varying opinions [9–11]. Additionally, from a computational perspective, merely modeling the individual loading event dynamics can be numerically expensive. Fully modeling this problem, when coupled with the many loading events (potentially millions), can be impractical.

One example of intermittent battery loading for MEMS devices, to be the focus of the case study in this paper, is that of switched piezoelectric or electrostatic MEMS actuation, both of which act as capacitive loads in terms of electrical behavior. This type of loading, especially when coupled with power electronics' dynamics, can have effects on multiple timescales as is shown in the conceptual schematics of a microrobot in Fig. 1 based on work in [12]. The authors have previously shown experimentally that useful battery lifetime when driving a capacitive load can have complex dependence on details of switching frequency, load capacitance, and various circuit current and switching losses [13]. From a modeling perspective, the authors have also shown that resulting battery behavior can be captured through adaptation of existing thin-film electrochemical models [2,3] through inclusion of additional switching and loading effects [14]. However, the accumulation of repeated individual loads created a dual-timescale problem when analyzing battery behavior over a complete discharge. In the earlier work, this was addressed by systematically perturbing system states, or changes in Li concentration at discretized points. In that manner, a numerical Jacobian or "transition matrix" could be developed describing changes in the system states over one fast-dynamic event. That transition matrix then could be used to approximate (or "project" over) multiple fast-dynamic events. This permitted simulation of battery discharge to be greatly accelerated, but simulation remained extremely computationally expensive and dependent on available hardware for parallelizing transition matrix development due to the large number of perturbations required. Furthermore, sources of accumulated error between the full model and accelerated simulation were not readily identifiable.

From a numerical methods perspective, the modeling and simulation of systems with disparate timescales is known to be challenging. Nonetheless, different approaches can be used depending on the specifics of the problem being analyzed. Engstler and Lubich presented an extrapolation approach where aspects of the problem are inactivated during portions of the extrapolation to reduce computation [15]. Constantinescu and Sandu extended this for "extrapolated explicit and implicit compound multirate steps" [16]. Roychowdhury discusses analysis of multiple time scale circuits by using different time variables [17]. Edwards shows an example approach with a heat conduction problem of two timescales [18]. A broad discussion on the topic of multiple timescales is given in [19].

Due to several features common to electrochemical battery modeling, the implementation approach of these traditional multi-scale methods may not be directly applicable. These aspects include: variable coefficients (seen in the concentration dependency of the diffusion coefficient), multiple timescale boundaries (slow evolving open circuit potential and fast switching dynamics), Neumann-type boundaries (positive electrode concentration), non-linear algebraic constraint of the boundary (exponential form of the Butler-Volmer equations), and the fact that the slow dynamics are produced due to accumulation of repeated fast dynamic events. While this does not preclude the possibility of adapting the above methods to the thin-film battery simulation problem examined here, this paper focuses on transition matrix methods as introduced above.

Here, we propose the use of intrinsic dynamics and numerical error analysis to model thin-film solid-state battery behavior over repeated fast timescale loading events in a computationally efficient form. First, we review the basic electrochemical battery model applied in previous work. Then, we describe how to directly compute a transition matrix for states of the discretized electrochemical model over fast timescale events using lithium concentration as the states of a dynamic system. This substantially reduces overhead in identifying the transition matrix relative to

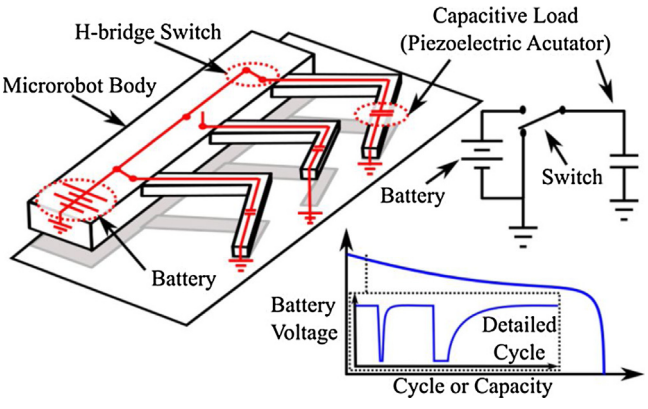

Fig. 1. MEMS micro-robot [12] switching and actuation schematics. A micro-robot schematic with a simplified equivalent circuit overlaid in red on the robot body is shown. A simplistic battery switching schematic, with an H-bridge (represented schematically as a simple single-pole double-throw switch) is shown, and similar simplistic switching was used in the case study here. A sample battery discharge profile is shown with a representative single capacitor charge cycle profile. (For interpretation of the references to colour in this figure legend, the reader is referred to the web version of this article.)

past work. Next, further understanding/improvement of projection of system states is achieved through an error analysis performed to decouple sources of error caused by approximations of various nonlinear phenomena that influence the state projections. In combination with knowledge of the expense of reducing certain error contributions, this allows for targeted error reduction. Finally, we demonstrate implementation of these modeling approaches in a case study looking at cyclic capacitive loading of a thin-film battery, arranged to mimic effects that might be seen in a microrobotic application [12,20,21]. The implementation of these modeling techniques is able to provide over a 44x reduction in function calls compared to our original approach [14] and a 99.96% computational reduction over a full simulation of the battery discharge, with additional savings possible with more aggressive updating and/or optimized time-stepping.

2. Modeling approach

2.1. Modeling nomenclature

Three main approaches to accelerated simulation of battery discharge are discussed in this paper, and will be referred to as follows. The approach from our prior work [14] that was based on perturbation of states, where the states were defined as changes in concentration, will be denoted as the "perturbed state approach." The current work develops a transition matrix that is developed directly from a modeled load and will be denoted as the "direct transition matrix approach." Additional improvements are made by targeted updates based on information gathered from the error analysis and this approach will be denoted as the "updating transition matrix approach."

In our prior work [14] we referred to the proposed type of loading as "cyclic capacitive" where "cyclic" refers to the repeated switching of a load (e.g. load on/load off), and "capacitive" refers to a load that behaves similar to an electrical capacitor. In common battery terminology "cycles" or "cyclic" generally refers to the full battery charge and discharge, additionally capacity and capacitance are easily confused. To avoid confusion, in this paper we will denote a single capacitive loading period (the actuator, represented by a capacitor, is charged and then discharged from the battery) as a "cap-cycle."

2.2. Modeling background

The foundation of our modeling approach is based on a one-dimensional electrochemical model of a thin-film battery presented in Fabre et al. [22] and others [1,3]. This was augmented based on the authors' findings in [13] to accommodate repeated cap-cycles [14]. A brief overview of the electrochemical equations will be given here. For a more through development, approximations, and assumptions, see the prior works [1–3,14]. The essence of the electrochemical model is a combination of the diffusion equation and boundary conditions describing the Li in the positive electrode, and a current balance through the battery based on the Butler-Volmer equation describing voltage changes at the electrolyte boundaries and Ohm's law describing the voltage drop across the electrolyte. This formulation is a partial differential equation (PDE) with Neumann boundary conditions, where one of those boundary condition is coupled algebraically to the voltage changes in the battery. The equations were nondimensionalized as noted in [14]. This gives us a nondimensional diffusion equation and boundary conditions for the positive electrode:

$$\frac{\partial \mathbb{Y}_+}{\partial \mathbb{T}} = \frac{\partial}{\partial \mathbb{X}}\left(\mathbb{D}(\mathbb{Y}_+)\frac{\partial \mathbb{Y}_+}{\partial \mathbb{X}}\right) \tag{1}$$

$$\frac{\partial \mathbb{Y}_+}{\partial \mathbb{X}} = f_1(\mathbb{I})|\mathbb{X} = 0 \tag{2}$$

$$\frac{\partial \mathbb{Y}_+}{\partial \mathbb{X}} = 0|\mathbb{X} = 1 \tag{3}$$

where the double struck charterers (e.g. $\mathbb{Y}_+$) symbolize a normalization or nondimensionalized value: $\mathbb{T}$ is time, $\mathbb{Y}_+$ is the concentration in the positive electrode, $\mathbb{X}$ is the spatial variable in the positive electrode, $\mathbb{D}(\mathbb{Y}_+)$ is the concentration-dependent diffusion coefficient in the positive electrode, and $\mathbb{I}$ is current which in part describes the positive electrode/electrolyte Neumann boundary condition. This current at the boundary needs to be balanced with the current through other parts of the battery using the Butler-Volmer equation which relates current and potential changes within the battery (electrode/electrolyte interfaces):

$$\mathbb{I} = f(\mathbb{Y}_e, \mathbb{Y}_+)[-\exp((\alpha_{a+} - 1) \times (\mathbb{V}_3 - \mathbb{V}_2 - \mathbb{U}))] \tag{4}$$

$$\mathbb{I} = g(\mathbb{Y}_e)[\exp(\alpha_{a-} \times -\mathbb{V}_1) - \exp((\alpha_{a-} - 1)\mathbb{V}_1)] \tag{5}$$

where f and g are functions of the current state of concentrations of the positive electrode ($\mathbb{Y}_+$) and electrolyte ($\mathbb{Y}_e$, approximated as constant); α_a is the anodic charge transfer coefficient with additional subscripts denoting the positive or negative electrode; $\mathbb{V}_1$,$\mathbb{V}_2$, and $\mathbb{V}_3$ are the voltages of the electrolyte at the boundary of the negative electrode, the voltage of the electrolyte at the positive electrode boundary, and the voltage of the positive electrode respectively; and $\mathbb{U}$ is the open circuit potential describing the battery potential at equilibrium for a given concentration in the positive electrode, and was determined from a combination of supplier data and experimental data. A basic schematic of the system setup is given in Fig. 2.

These equations were implemented with a combination of optimization and finite difference approaches to converge on currents and concentrations in the battery as suggested by Fabre et al. [22], with implementation aided by additional numerical method techniques from [23] and [24]. Additional approximations included by Fabre, and retained in our model include: no potential drop in the negative electrode, constant conductivity in the electrolyte, and no self-heating effects. Additionally we treat the positive electrode as a perfect electrical conductor so no voltage drop occurred. For simplicity the diffusion coefficient was based on the concentration of the previous time step, removing the time dependency.

The model in the non-dimensional form comes down to nine key parameters as noted in [14]. These parameters can be summarized as: one describing the characteristic time of the diffusion, one describing the positive electrode current and capacity, five that involve the electrolyte and electrode/electrolyte interface, one characterizing the parasitic capacitance, and one characterizing losses in the switching circuit. The approach for calibration is currently to iteratively step through calibration with subsets of the parameters, with potential for improvement and extension to determine changes over battery life.

Due to the fast changes that can take place in repeated cap-cycles, it may be necessary to discretize with very fine time steps during certain periods in the finite difference approach.

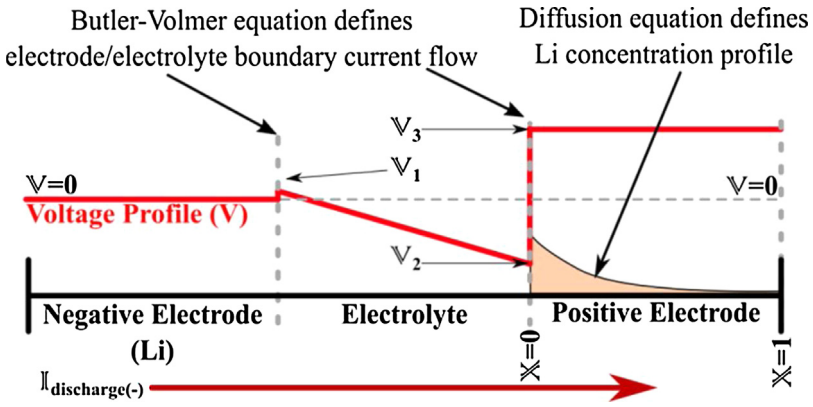

Fig. 2. Battery model schematic. The one-dimensional battery model is shown with the voltage and spatial locations. The corresponding equations are indicated. Adapted from [14].

Numerically, the result of these fast dynamics is an increase in numerical expense for solving a single cap-cycle. This becomes problematic when extending the modeling to long periods of time, where it is not realistic to perform detailed modeling for all cap-cycles. Therefore an approach for taking current system states and being able to project these over many repeated cap-cycles in the future is of great interest.

2.3. Projection modeling: direct transition matrix approach

Various sets of system quantities can be used as states of a dynamic system. The "perturbed state approach" used changes of concentration in the positive electrode ($\Delta\mathbb{Y}_+$) as states of the system and was presented by the authors with the basic switching model in [14]. This projection approach used perturbation of the concentration changes at each finite difference grid point of the positive electrode independently to build a numerical Jacobian or transition matrix. One major limitation of this approach was the necessity to perturb the system for each grid point. This burden can be reduced through parallel processing. However, it was determined that if a change was made to the state definition, then the transition matrix could be developed directly from the model without the need of perturbations. Instead of using the change in concentration, $\Delta\mathbb{Y}_+$, as the states of the system, the concentrations themselves, $\mathbb{Y}_+$, were used. The transition matrix associated with these states then becomes the accumulated finite difference steps during each cap-cycle. This change may seem insignificant, yet as will be seen can have important implications for computational efficiency.

The basic development of the new transition matrix is presented here. The positive electrode lithium concentration profile calculated by the finite difference is a function of the current and diffusion coefficient. The current dictates the boundary condition and all points are functions of the diffusion, which in turn is dependent on the concentration (for simplicity the diffusion coefficient was based on the concentration of the previous time step). The finite difference approach in concentration used to solve Eqs. (1)–(3), can be expressed as:

$$\mathbf{A}_{i,n}\mathbb{Y}_{\mathrm{i,n+1}} = \mathbf{B}_{i,n}\mathbb{Y}_{\mathrm{i,n}} + \mathbf{r}_{i,n} | \mathbf{A},\mathbf{B} = f(\mathbb{D}) and \mathbf{r} = g(\mathbb{I},\mathbb{D}) \tag{6}$$

where $\mathbb{Y}_{\mathrm{i,n}}$ is the concentration profile vector in the positive electrode at time step "*n*" of cap-cycle "*i*." Matrices **A** and **B** are functions of the diffusion coefficient and **r** incorporates the boundary conditions for the given time step including the information about the flux (based on the electrical current) and the diffusion coefficients at the boundary.

The implementation of this in practice was done using a combination of information from [23] and [24], with the finite difference matrices set up as follows to account for a non-uniform mesh. For a 1D mesh of N + 1 grid points, let h_k be the distance between grid point k and $k+1$, $\mathbb{D}_k$ be the diffusion coefficient of the grid point (based on the concentration from the last time step), and τ the time step size. We can then define:

$$p_k = \frac{h_k^2}{4h_{k-1}^2}\mathbb{D}_{k-1} + \frac{3h_{k-1}^2 + 2h_{k-1}h_k - h_k^2}{4h_{k-1}^2}\mathbb{D}_k - \frac{1}{4}\mathbb{D}_{k+1} \tag{7}$$

$$r_k = \frac{1}{4}\mathbb{D}_{k-1} + \frac{-h_{k-1}^2 + 2h_{k-1}h_k + 3h_k^2}{4h_k^2}\mathbb{D}_k - \frac{h_{k-1}^2}{4h_k^2}\mathbb{D}_{k+1} \tag{8}$$

$$q_k = -(p_k + r_k) \tag{9}$$

$$s_k = \frac{(h_{k-1} + h_k)^2}{2\tau} \tag{10}$$

We then can build the inner parts of the **A** and **B** matrices from (6):

$$\begin{array}{l} \mathbf{A}(k,k-1) = -p_k \\ \mathbf{A}(k,k) = s_k - p_k \\ \mathbf{A}(k,k+1) = -r_k \\ \mathbf{B}(k,k-1) = p_k \\ \mathbf{B}(k,k) = s_k + p_k \\ \mathbf{B}(k,k+1) = r_k \end{array} \tag{11}$$

Using ghost points we address the diffusion coefficient at the boundaries,

$$C = \frac{2h_1^2}{\tau} \tag{12}$$

$$\begin{array}{ll} \mathbf{A}(1,1) = \mathrm{C} + 2\mathbb{D}_1 & \mathbf{A}(1,2) = -2\mathbb{D}_1 \\ \mathbf{A}(N+1,N) = -2\mathbb{D}_{N+1} & \mathbf{A}(N+1,N+1) = \mathrm{C} + 2\mathbb{D}_{N+1} \\ \mathbf{B}(1,1) = \mathrm{C} - 2\mathbb{D}_1 & \mathbf{B}(1,2) = 2\mathbb{D}_1 \\ \mathbf{B}(N+1,N) = 2\mathbb{D}_{N+1} & \mathbf{B}(N+1,N+1) = \mathrm{C} - 2\mathbb{D}_{N+1} \end{array} \tag{13}$$

Finally, to incorporate the Neumann boundary conditions we convert the value to a Dirichlet condition for that time step to build the **r** vector from (6), which is zero except the first element.

$$\mathbf{r}(1) = \mathbb{D}_{N+1} \tag{14}$$

With the finite difference matrices formulated we can then incorporate the boundary condition information in **r** with **B** such that (6) is rewritten as:

$$\mathbb{Y}_{i,n+1} = \mathbf{A}_{i,n}^{-1}\mathbf{B}_{i,n}^{*}\mathbb{Y}_{i,n} | \mathbf{B}^{*} = f(\mathbb{I}, \mathbb{D}, \mathbb{Y}_{i,n}) \tag{15}$$

If $\mathbb{I}$, current, and $\mathbb{D}$, diffusion coefficient, are known at each time step in a cycle, the matrices **A** and **B** can be determined directly. Thus, the full cycle transition matrix $\mathbf{\Phi}$ can be calculated as:

$$\mathbb{Y}_{i+1,1} = \mathbf{\Phi}_{i}\mathbb{Y}_{i,1} = \left(\prod_{j=1}^{n}\boldsymbol{A}_{i,j}^{-1}\boldsymbol{B}_{i,j}^{*}\right)\mathbb{Y}_{i,1} \tag{16}$$

This allows us to create the transition matrix from a single cap-cycle as a composite of all the finite difference steps. If we assume that the transition matrix is approximately constant over the projection of *m* cap-cycles, then, as in the perturbed state approach, we have:

$$\mathbb{Y}_{i+m,1} = (\mathbf{\Phi}_{i})^{m}\mathbb{Y}_{i,1} \tag{17}$$

This enables one to use the transition matrix from a single cap-cycle to project over many cap-cycles similar to the perturbed state approach. Performing the calculations this way allows us to get an approximation of the states throughout the projection without needing to solve the algebraic component created by the Butler-Volmer equations, which is a critical source of computational complexity in this type of problem. Additionally, depending on hardware, this approach can have significant overhead reduction compared to the perturbed state approach.

There are two main limitations to this approach. First, as with the prior approach, we assume a constant transition matrix over the projection, which in essence approximates no changes in cap-cycle current and diffusion coefficients profiles over the projection, as well as certain aspects of the boundary concentration information. This assumption will likely be the main limitation in size of projection that can be made for a given permissible error, and will have varying effects dependent on the nonlinearities and loading of the system. Second, by defining the system states as the concentration levels, instead of differential concentration as in our previous work [14], we may reduce the sensitivity due to numerical round off error. However, loss in sensitivity can be outweighed by decreased numerical expense in our current application.

2.4. Error analysis

Since a major limiter to the projection size is the error caused by the approximation of a constant transition matrix over the full projection, understanding the severity of various components of this error provides insight for its mitigation. Therefore, here we performed a detailed error analysis of the assumptions related to a constant transition matrix. To frame this analysis we need to revisit the formulation of the direct projection transition matrix,

$$\mathbb{Y}_{i,n+1} = \mathbf{A}_{i,n}^{-1}(\mathbf{B}_{i,n}\mathbb{Y}_{i,n} + \mathbf{r}_{n}) = \mathbf{A}_{i,n}^{-1}\mathbf{B}_{i,n}^{*}\mathbb{Y}_{i,n}. \tag{18}$$

In the first part of the equation $\mathbf{r}_{n}$ is independent of $\mathbb{Y}$; however, to bring this boundary condition information into the transition matrix, $\mathbf{r}_{n}$ is incorporated into $\mathbf{B}^{*}$ resulting in $\mathbf{B}^{*}$ necessarily becoming coupled with the concentration $\mathbb{Y}$ around the boundary. We can rewrite (18) as

$$\mathbb{Y}_{i,n+1} = \mathbf{A}_{i,n}^{-1}(\mathbf{B}_{i,n} + \mathbf{r}_{n}^{*})\mathbb{Y}_{i,n} | \mathbf{r} = f(\mathbb{I}_{i,n}, \mathbb{D}_{i,n}, \mathbb{Y}_{i,n}) \tag{19}$$

where $\mathbf{r}^{*}$ assumes the dependence on $\mathbb{Y}$ around the boundary. If we assume N finite difference steps for one full cap-cycle, we can then express the concentration changes over the entire cap-cycle as:

$$\begin{aligned}\mathbb{Y}_{i,N+1} &= \mathbb{Y}_{i+1,1}\\ &= \mathbf{A}_{I,N}^{-1}\left(\mathbf{B}_{I,N} + \mathbf{r}_{I,N}^{*}\right)\ldots\mathbf{A}_{I,1}^{-1}\left(\mathbf{B}_{I,1} + \mathbf{r}_{I,1}^{*}\right)\mathbb{Y}_{I,1}\\ &\qquad |\mathbf{A}, \mathbf{B} = f(\mathbb{D}); \mathbf{r}^{*} = f(\mathbb{I}, \mathbb{D}, \mathbb{Y})\\ &= \prod_{j=0}^{N-1}\left\{\mathbf{A}_{i,N-j}^{-1}\mathbf{B}_{i,N-j} + \mathbf{A}_{i,N-j}^{-1}\mathbf{r}_{N-j}^{*}\right\}\mathbb{Y}_{i,1}\\ &= \mathbf{\Phi}_{i}\mathbb{Y}_{i,1}\\ &\qquad |\mathbf{\Phi}_{i} = f(\mathbb{I}, \mathbb{D}, \mathbb{Y})\end{aligned} \tag{20}$$

Here we see that the transition matrix $\mathbf{\Phi}$ is in reality a function of the current profile during the cap-cycle, $\mathbb{I}$, the diffusion coefficient, $\mathbb{D}$, and the concentration $\mathbb{Y}$ around the boundary. Using the projection approaches described previously, $\mathbf{\Phi}$ is approximated as constant over the projection. The error associated with this simplification can be divided into three main components. First is error due to changes in the diffusion coefficient in the main bulk of the electrode. This is caused by the concentration dependence of the diffusion coefficient and comes from errors associated with the $\mathbf{A}^{-1}$ and **B** matrices. Second is error due to the changes in the current profile from one cap-cycle to the next. Third is error associated with changes in concentration and diffusion at the boundary. This accounts for the diffusion and concentration dependency of $\mathbf{r}^{*}$. If we assume that the transition matrix is based on some earlier cap-cycle "*O*," we can define these errors as follows:

$$\begin{aligned}\mathbf{E}_{A^{-1}:i,n} &= \mathbf{A}_{O,n}^{-1} - \mathbf{A}_{i,n}^{-1}\\ \mathbf{E}_{B:i,n} &= \mathbf{B}_{O,n} - \mathbf{B}_{i,n}\\ \mathbf{E}_{r^{*}:i,n} &= \mathbf{r}_{O,n}^{*} - \mathbf{r}_{i,n}^{*}\end{aligned} \tag{21}$$

where $\mathbf{E}_{A^{-1}:i,n}$ is the error or difference between the values of $\mathbf{A}^{-1}$ in the current cap-cycle "*i*" and time step "*n*", $\mathbf{A}^{-1}$ of time step "*n*" for the earlier cap-cycle "*O*" on which the projection transition matrix is based. Similarly with $\mathbf{E}_{B:i,n}$ and $\mathbf{E}_{r^{*}:i,n}$. The error $\mathbf{E}_{r^{*}:i,n}$ is a combination of $\mathbf{E}_{\mathbb{I}:i,n}$, the error associated with the change in the current profile, and $\mathbf{E}_{\mathbb{B}:i,n}$, the error associate with the boundary concentration and diffusion,

$$\mathbf{E}_{r^{*}:i,n} = \mathbf{E}_{\mathbb{I}:i,n} + \mathbf{E}_{\mathbb{B}:i,n} \tag{22}$$

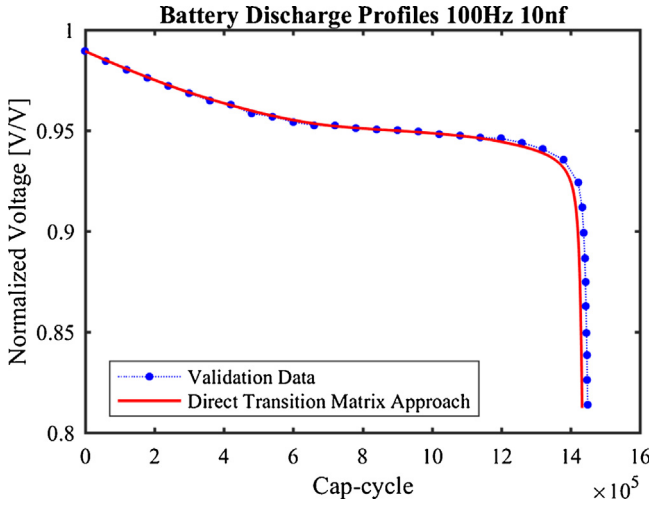

Fig. 3. Model and validation data comparison full battery discharge. Validation data is averaged unlike that shown in [14].

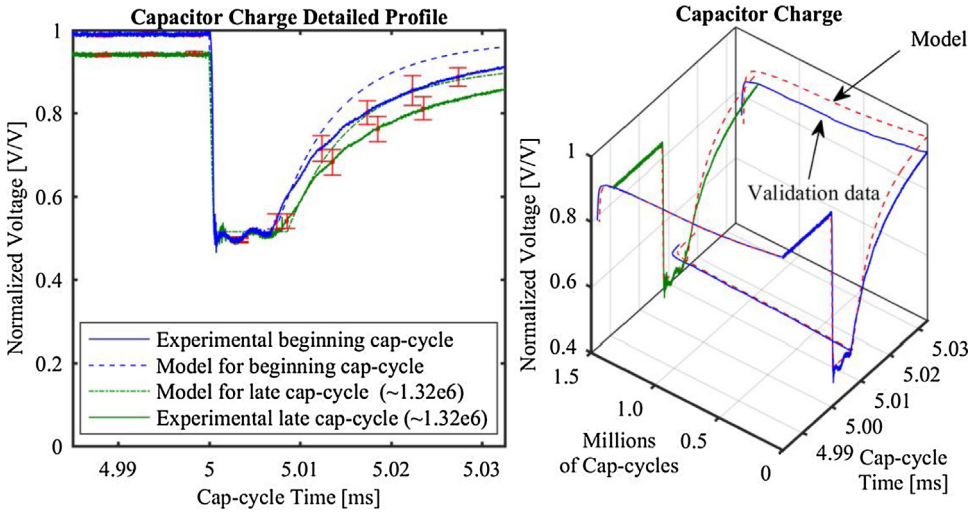

Fig. 4. (Left) Model and validation data comparison of a detailed capacitor charge profile. Error bars show error from rolling average and from discrepancy between battery and capacitor voltage readings. (Right) The validation and model data are presented with just key features showing the fit in select cycles and over the full battery discharge. Error bars are omitted from the experimental data.

Using this we can generalize and rewrite Eq. (20) as:

$$\mathbb{Y}_{i+1,1} = \left\{ f\left(\mathbf{A}_O^{-1}, \mathbf{B}_O, \mathbf{r}_O^*\right) - f\left(\mathbf{A}_O^{-1}, \mathbf{B}_O, \mathbf{r}_O^*, \mathbf{E}_{A^{-1}:O}, \mathbf{E}_{\mathbf{B}:O}, \mathbf{E}_{\mathbb{I}:O}, \mathbf{E}_{\mathbb{B}:O}\right) \right\} \mathbb{Y}_{i,1} \tag{23}$$

A more thorough formulation of this expression can be done, but does little here to further the topic so will not be presented. Details of the findings will be given later.

2.5. Projection modeling: updating transition matrix approach

Ultimately our goal is to be able to model these systems in an accurate, numerically reasonable way. The ability to analyze the error and to separate the various components and interactions is extremely helpful in determining potential error reduction strategies. If at select steps in the projection we could update the transition matrix with real or approximated values, we could potentially lengthen the projection and/or reduce the error. Some key considerations are as follows: first, updating $\mathbb{B}$, $\mathbb{D}$, and $\mathbb{I}$ of a step during the projection would in essence be similar to running a full model and would essentially eliminate error (and give no numerical savings); second, updating $\mathbb{I}$ is numerically expensive in that we need to calculate the Butler-Volmer equations for each time step of the cap-cycle to gather that information, which is likely comparable to performing the full model; third, updating $\mathbb{D}$ and $\mathbb{B}$, can be done at a lower numerical cost because an approximation at each time step can be determined without needing to solve the algebraic aspects of the Butler-Volmer equations. Using these considerations and outcomes from the error analysis we implemented a transition matrix updating method where key aspects of the transition matrix are adjusted at certain points in the projection.

3. Case study: thin-film battery loading

With a modeling approach fully developed, it is instructive to see this technique demonstrated in a case study. As mentioned previously, one problem of interest for this type of modeling is loading of thin-film batteries with repeated capacitive loads, such as what could be seen in certain microrobot applications [12,21,25]. For example, walking gaits for a piezoelectric microrobot requires repeated charging of piezoelectric actuators that behave electrically as capacitive loads. The modeling incorporated findings based on a simplistic switching approach from the authors' in [13] to accommodate repeated cap-cycles and the perturbed state approach in [14]. This application can see fast current and voltage changes at times, necessitating fine discretization during certain time periods in the finite difference approach. Using the approaches mentioned here for taking current system states of the battery and being able to project these over many repeated cap-cycles in the future is of great importance. For a given permissible error in projection, projection lengths will need to be shorter later in the battery discharge as non-linearities increase, as seen in part in the battery discharge profile sketch in Fig. 1. For this case study, permissible errors were set and simple algorithms implemented to determine projection size.

It is worth noting also that the given load scenario of the case study in this and prior modeling work by the authors is a light load and it has been determined that simpler underlying battery models could be used with equal validity. However, the electrochemical model presented here gives a broader range of applicability than simpler models do (such sceneries have been identified) and allows for more direct parameter correlation, such that the

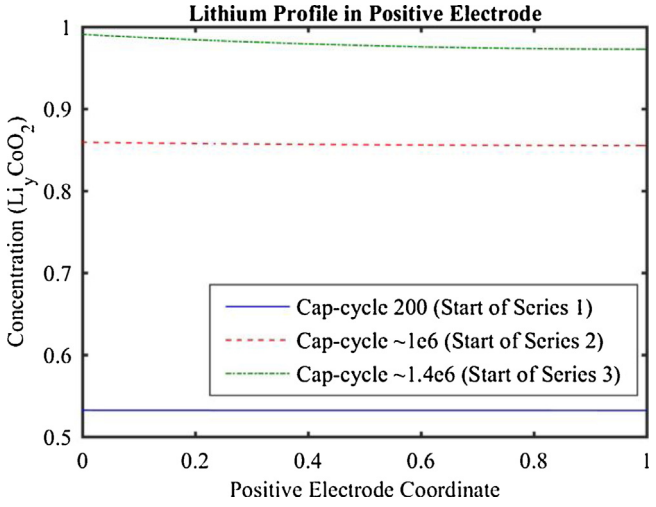

Fig. 5. Lithium profile in the positive electrode at the beginning of the three projections for error analysis.

modeling concepts and approaches presented are considered valid and useful. Some minor issues with the model implementation were addressed for the two new approaches presented here, and the current implementation shows some limitations at times when the battery has low loads on the order of the leakage current of the circuit that cause some numerical oscillations, but these issues are minor.

3.1. Experimental data acquisition

Experimental testing was performed previously, for calibration and validation, to simulate a load profile similar to a cycled piezoelectric actuator, using a standard capacitor (constant current discharges were also used in calibration). The batteries used for experimental testing were 50 μAh thin-film lithium batteries from Cymbet™ [26]. These batteries had a chemistry that would potential be suitable for microrobotic applications, although form factor and other aspects of off-the shelf batteries is not currently compatible. It appears that these may be "Li-free" batteries, meaning the lithium negative electrode is likely plated on the current collector during the first charging of the battery rather than an ideal lithium source, yet our modeling still appears adequate. Model calibration and initial results were published in [14]. Detailed description of the limitations in the data is given in [13,14], however four main general points will be noted. First, the current measurement for the cycled tests was measured with an AC probe and converted to a DC reading with accuracy limited by the conversion approach. Second, substantial noise and extraneous effects in the cycled data had to be addressed. Third, the testing was performed with multiple batteries, so some variability was introduced. Fourth, constant current data used for calibration, which reported lower capacities then the published data sheet, was linearly scaled to correspond with those of the calibration switching data set based on an equivalent current in attempt to account for differences in dataset acquisition/assumptions and ultimately to align assumed comparable capacity usage [14]. It is unclear why the constant current data would be further from the published data values when it was taken with a more straightforward measurement approach. Because of these limitations, the data here is used more for model approach validation rather than for use as precise experimental result presentation. Representative profiles of the switching dynamics will be shown later.

3.2. Direct transition matrix approach

From the validation dataset, the starting voltage is input into the model as an initial condition (all other information comes from the calibration). This starting voltage measurement is influenced by the leakage current, and is accounted for in the model as before [14]. An algorithm was developed to determine projection size based on permissible errors. Projections ranged from 100 to 40,000 cap-cycles, with more aggressive projection possible. A certain number of fully simulated cap-cycles after each projection were generally added to allow the model to settle. Projections began after the 200th cap-cycle, where projections began after the 300th cap-cycle in the perturbed state approach.

The overall discharge profile of the battery validation dataset [14] and the direct transition matrix approach are shown in Fig. 3 and show good agreement. In addition to the overall battery discharge profile, comparison was made between experimental data and the direct transition matrix approach for detailed profiles of the capacitor charge. Two sample charge profiles are given in Fig. 4, and are combined with the overall discharge profile to represent the fit of the model and validation data over time. This fitting of the individual cycles is comparable to the perturbed state approach.

3.3. Error quantification

Quantification of errors caused by approximations during projection is desirable for targeting modeling improvements. One simplistic method of error quantification is through performing comparison between full modeling of a series of cap-cycles and an associated projection over the same series. This preliminary error quantification was performed for three separate series in the modeled battery discharge that represent three key regimes. The first series begins near cap-cycle 200 of the discharge, where nonlinear affects are low. The second series begins near 1e6 cap-cycles, which still has low nonlinearities in the open circuit potential profile but is in the range where diffusion coefficients are changing. The final series begins near 1.4e6 cap-cycles. Here, there are significant nonlinearities and the error grows quickly with projection size. Each of these three series were fully simulated for 1000 cap-cycles, and a corresponding projection was also calculated over the same period.

Two aspects of the error seen between the fully simulated cap-cycles and the projected cap-cycles are of interest. First is the

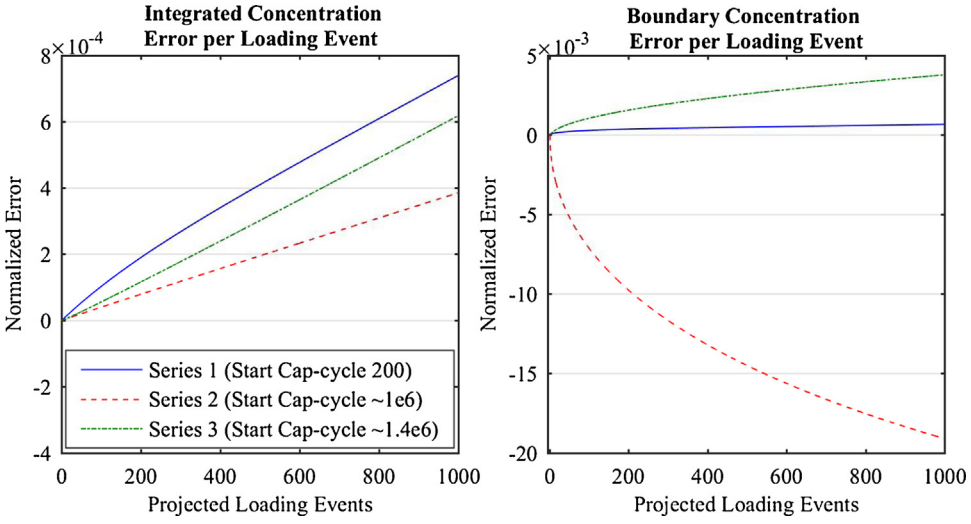

Fig. 6. (Left) Integrated concentration error per cap-cycle for three separate projections. (Right) Boundary concentration error per cap-cycle for three separate projections.

boundary condition $\mathbb{Y}_+(0)$, the normalized lithium concentration at the positive electrode/electrolyte boundary, which is approximated to range from 0.5 if a battery is fully charged to 1 V/V and 1 at fully discharged. This boundary influences the voltage of the electrode as well as indicates when the battery is fully discharged. Second is the integrated area of the lithium concentration profile in the positive electrode. This is an expression of the amount of capacity used, and conversely, the amount of capacity left in the battery. The lithium profiles across the positive electrode at the beginning of the three projections are shown in Fig. 5. For faster switching (higher average current) and for lower diffusion coefficients, the profiles would show more variation across the electrode.

For each of the three series, the error over the 1000 cap-cycles was calculated as the difference between the normalized lithium concentration in the positive electrode, $\mathbb{Y}_+(0)$, of the direct

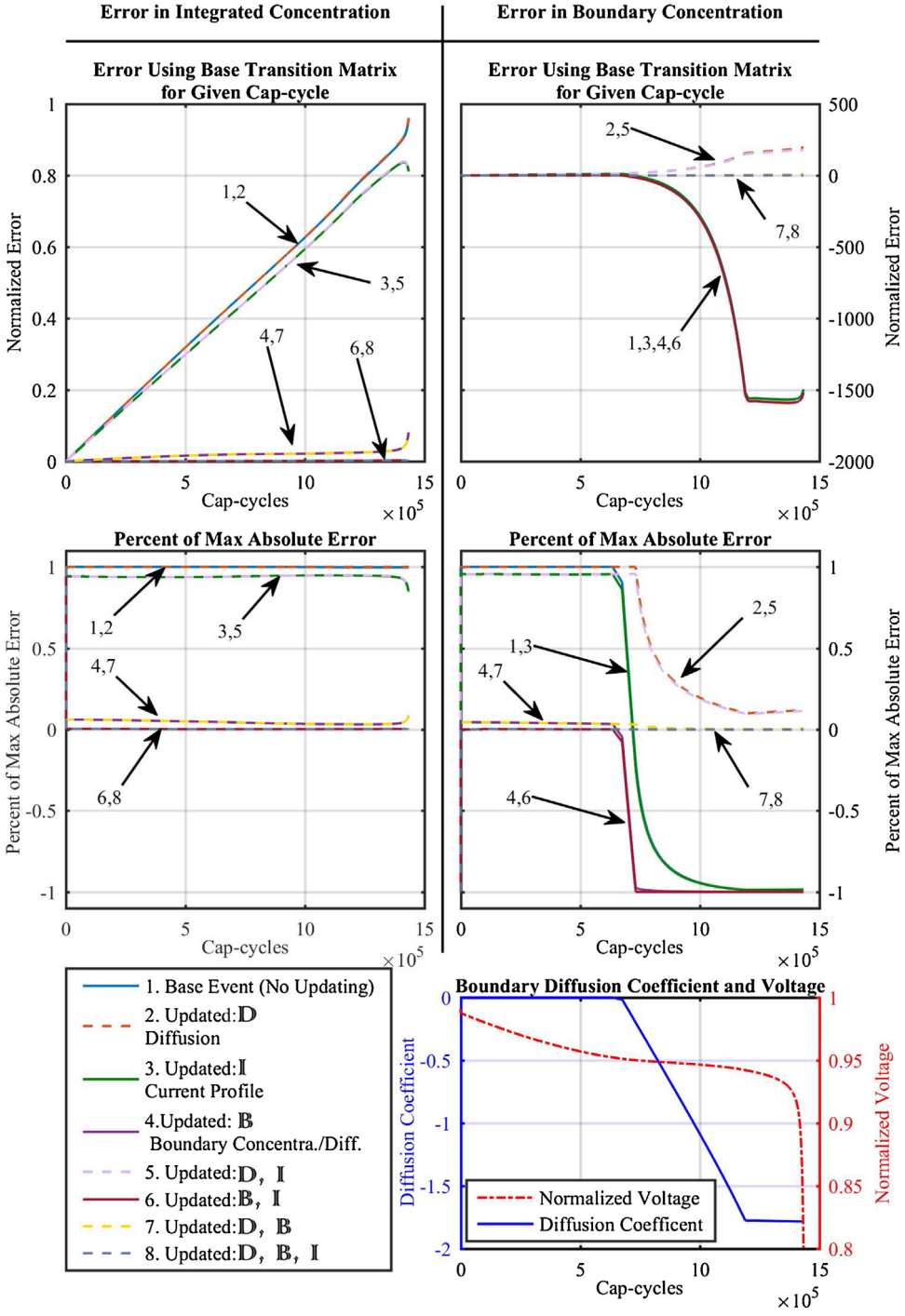

Fig. 7. Error analysis results. Errors associated with using information from the base (10th) cap-cycle to calculate the concentration change for the given cap-cycle compared to the full modeling of that cap-cycle. (Left) Error in the boundary concentration. (Right) Error in total integrated concentration. (Top) Error for the given scenarios normalized by the change in concentration of the 200th cap-cycle. (Middle) Ratio of the error for each scenario compared to the maximum absolute error of any scenarios for the given cap-cycle. (Bottom-Right) The boundary diffusion coefficient and voltage, given for references to see the nonlinearities introduced.

projection method and the fully simulated series results (i.e. no projections over the 1000 cap-cycles).

This error was then normalized by the change in concentration of cap-cycle 200. This means that the errors presented indicate approximately the fraction of the change seen in one regularly modeled cap-cycle. The errors per cap-cycle are given in Fig. 6.

It can be seen that the error for the boundary concentration is quite low for series 1, yet is much higher for series 2 and 3 where there are significant nonlinearities. However, for the integrated concentration the errors are more similar, and the first series actually showing slightly more error than the others. These plots suggest that understanding of the error contributions over time could potentially improve the accuracy of the projection, and/or allow for larger projections or decreased numerical expense.

In light of this, a more thorough error analysis was performed, as described in Section 2.4. The key feature of the error is that the different components contribute to the combined error at different times and in different ways. To further understand these different components we selected a reference cap-cycle near the beginning of the full battery discharge (10th cap-cycle) as a base.

Using notation from Eqs. (18) and (23), we can develop the **A** and $\mathbf{B}^*$ matrices for all the steps in this base cap-cycle. These matrices combined can form the base transition matrix.

In order to compare different components of the error, we adjusted these base **A** and $\mathbf{B}^*$ matrices in several ways for each cap-cycle modeled. It should be noted that the cap-cycles modeled in this error analysis are a large subset of the cap-cycles fully modeled during the direct transition matrix approach. For each cap-cycle analyzed we used the concentration profile determined in the direct transition matrix approach, previously presented, as the beginning concentration for the cap-cycle. Then the changes associated with that cap-cycle were calculated in the following way: First, the concentrations were calculated solely using the base matrices (Base). Second, these base matrices were adjusted to

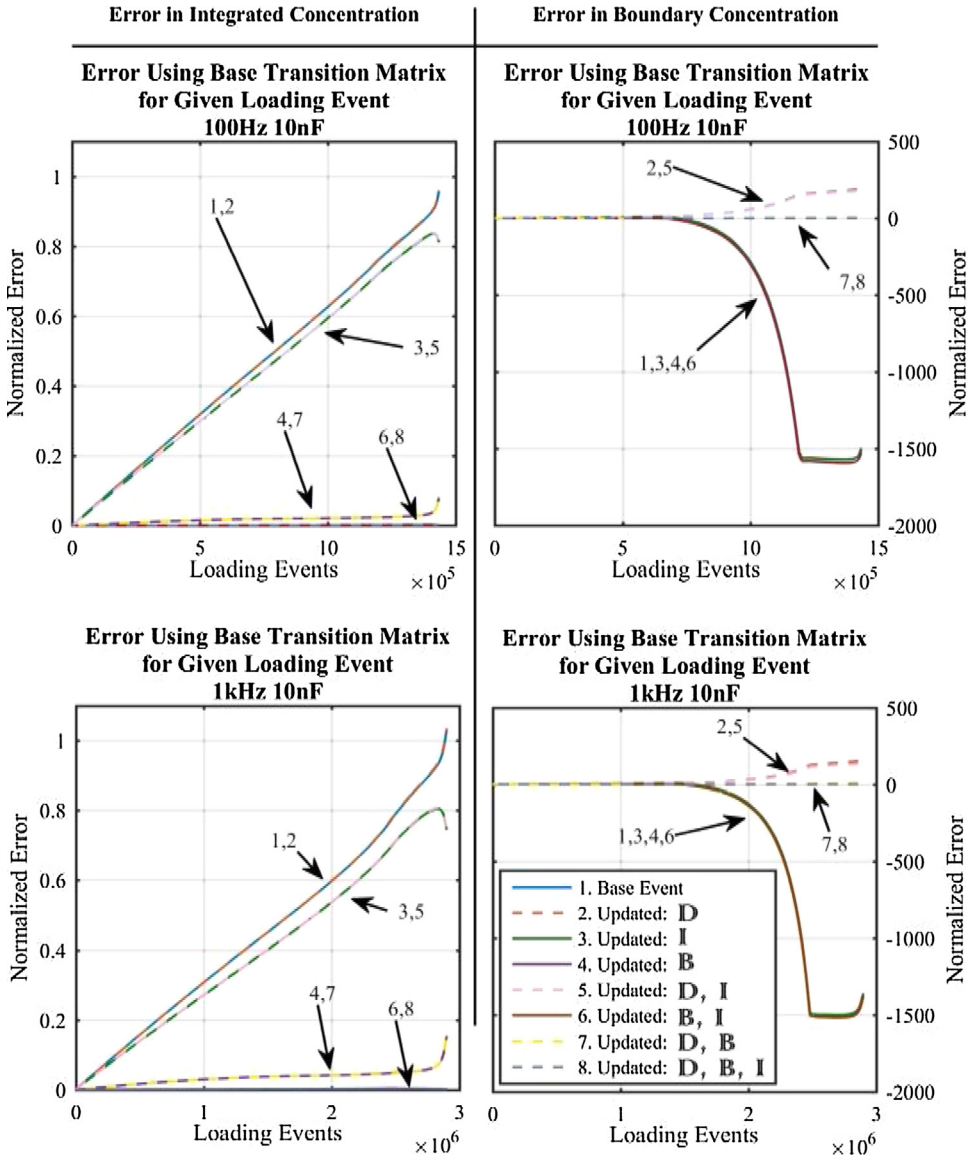

Fig. 8. Error analysis plots for (Top) 100 Hz 10 nF for comparison (Bottom) 1 kHz 10 nF load. Errors associated with using information from the base (10th) cap-cycle to calculate the concentration change for the given cap-cycle compared to the full modeling of that cap-cycle. (Left) Error in the boundary concentration. (Right) Error in total integrated concentration. Error for the given scenarios are normalized by the change in concentration of the 200th cap-cycle.

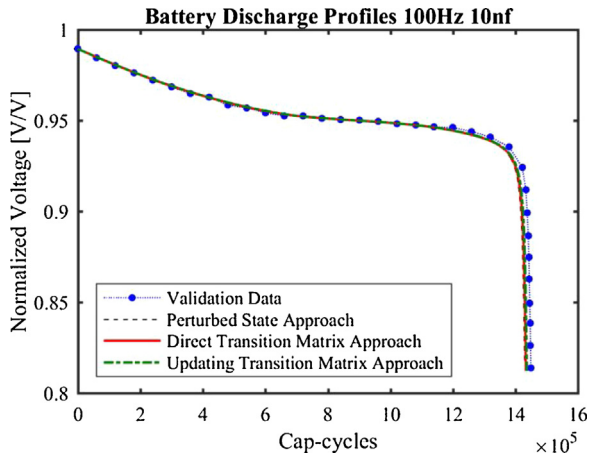

Fig. 9. Comparison of the updating transition matrix approach with the direct transition matrix approach, experimental data and the perturbed state approach in [14]. Validation data is averaged unlike that shown in [14].

account for diffusion coefficient difference in the bulk of the positive electrode, thus removing that error component ($\mathbb{D}$). Third, the base matrices were adjusted to account for the current profile difference, thus removing that error component ($\mathbb{I}$). It should be noted that the current profiles used to update the matrices were from those stored during the full modeling, as these are not readily available without fully modeling the cap-cycle. Fourth, the base matrices were adjusted to account for boundary concentration and diffusion differences, thus removing that error component ($\mathbb{B}$). Combinations of these adjustments were also performed. Because the discretization in time for each cap-cycle was not necessarily equal from cap-cycle to cap-cycle, linear approximations of some values were made when applying data from one cap-cycle to another. Finally these were compared to the fully modeled cap-cycle obtained when running a full direct transition matrix approach. The error then became the difference between the concentration profile change in the fully modeled cap-cycle and the profile developed using the base and augmented matrices. The error between each approach and the fully modeled cap-cycle was normalized by the change in concentration of the 200th cap-cycle, as before. Boundary and total integration concentration errors are presented in Fig. 7. Upper plots of Fig. 7 show the normalized error.

The middle two plots show a ratio of the error for each adjustment approach compared to the maximum absolute error seen in any of the adjustment approaches (including no adjustment, or the base transition matrix) for the given cap-cycle. Finally, in the bottom right the boundary diffusion coefficient and voltage are given for reference to help visualize nonlinearities being introduced into the system.

The overall error plots (top two plots) give an understanding that the magnitude of the boundary error is significantly larger than that of the total concentration error. Although not distinguishable in this plot, this is true for earlier loading events, but at a smaller magnitude difference. Additionally, it is striking that the total concentration error has a nearly linear rise compared to the non-linear boundary error. Finally, the total concentration error seems little affected by the changing diffusion coefficient and more affected by the voltage profile, whereas the boundary seems affected by both. This last point compliments the determination of which updating method gives the greatest improvement. For both types of error the best results are when updating is done for all three components, however if only updating two of the three, the best updating approach is different for the boundary or total concentration error (total concentration is benefited by the updating $\mathbb{I}$ and $\mathbb{B}$, and boundary concentration is benefited most by updating the $\mathbb{B}$ and $\mathbb{D}$). Combining these we can state that the total concentration error is most affected by changes in the electrical aspects of the system, that is current and voltage. Whereas the boundary concentration error is more affected by changes in the diffusion and boundary concentration. However, if we were to switch those, the effect of updating only $\mathbb{I}$ and $\mathbb{B}$ has a much more adverse effect on the boundary concentration than updating only $\mathbb{B}$ and $\mathbb{D}$ has on the total integrated concentration. Understanding this can allow error reduction in a more systematic way.

For comparison, the same approach was used for a reduced number of cap-cycles for a 1 kHz 10 nF loading, and the plots of the normalized error are shown in the bottom plots of Fig. 8. It can be seen that very similar error occurs at this elevated loading.

3.4. Updating transition matrix approach

Using the information gathered from the error analysis we implemented a transition matrix updating method. For each projection, at five points during the projection the transition matrix was updated using current approximations of $\mathbb{D}$ and $\mathbb{B}$. Then if n_i is the ith update for a projection of m cap-cycles and $\mathbf{\Phi}^*_{n_i}$ is the updated transition matrix using the intermediate values of $\mathbb{Y}_{i+n_i,1}$ to update diffusion coefficients and boundary conditions, we have

$$\begin{aligned} 1,2,\ldots,n_1-1,n_1,n_1+1,\ldots,n_i,\ldots,\mathrm{m} \\ \mathbb{Y}_{i+n_1,1} &= \left(\mathbf{\Phi}_\mathrm{i}\right)^{n_1}\mathbb{Y}_{i,1} \\ &\vdots \\ \mathbb{Y}_{i+m,1} &= \left(\mathbf{\Phi}^*_{n_x}\right)^{N-n_x}\mathbb{Y}_{i+n_x,1} \end{aligned} \tag{24}$$

In this way the transition matrix has some approximated updating during the projection to increase fidelity. The numerical cost for the combined five updates was equivalent to about one regular function call or cap-cycle.

3.5. Approach comparison

The overall discharge profile of the battery validation dataset and the perturbed state approach [14] is compared to the two projection approaches presented here and is shown in Fig. 9. It can be seen that there is close agreement with all approaches.

To compare the numerical costs between the perturbed state approach and the approaches reported here it is useful to look at the number of cap-cycles fully modeled (or equivalent function calls) compared to the total number of cap-cycles modeled (including projections). To perform this calculation, certain approximations had to be made as to how to deal with overhead and parallel processing. It is understood that this is not a perfect comparison between the three approaches in that the some

Table 1
Computational Expense for Various Projection Approaches.

Transition Matrix Approach	Total Loading Events	Function Calls	Approx. Function Time [hr]	Numerical Cost
Perturbed	1.430e6	90510	75.4	6.3%
Direct	1.430e6	6558	5.5	0.46%
Updating	1.430e6	2038	1.7	0.14%

variations existed between the methods (e.g. number of cap-cycles before projections began, parallel processing, overhead, and allowed error algorithm variation), but the comparison is still considered instructive.

For the given hardware and permissible error algorithms used, the direct approach had a numerical cost of 0.08% (equivalent function calls/total cap-cycles) after ~0.74 million cap-cycles and 0.46% after ~1.43 million cap-cycles where the updating approach was only 0.14% after ~1.43 million cap-cycles. This may be compared to our previous approach, the perturbed state approach, with states of differential concentration [14], which reported a cost of 0.19% after ~0.677 million cycles, and 6% after ~1.43 million cycles. A comparison of the three projection transition matrix approaches is given in Table 1 where the numerical expenses are compared with representative times.

It is acknowledged that costs will vary depending on hardware, assumptions of overhead etc., and with acceptable error algorithms, however, these findings highlight potential gains for the direct and updating approaches. Times were based strictly off of an approximate 3 s per function call which is a reasonable approximation for demonstration. The length of this function call is important to highlight for two reasons. First, the time stepping approach within each cycle was not optimized and improvement could be made in future work in the time required. Second, even with significant improvements in function call time, due to the large number of total cap-cycles per test, any appreciable function call time will likely necessitate model reduction methods. A final note is that the computation time for the updating transition matrix approach in this modeling scenario, was less than the experimental run-time, thus suggesting potential pseudo-real time applications.

4. Conclusions

Prior work by the authors aimed at exploring the potential of modeling systems with repeated capacitive loading, in particular for MEMS applications. This prior work combined switching and battery dynamics to explore the effects of this type of loading on a potential battery system. However, numerical expense of one capacitive load event (cap-cycle) was significantly numerically intensive to preclude reasonable modeling of the proposed full system. Therefore, a projection approach was presented in that work to reduce this expense by projecting system states over large series of consecutive cap-cycles. This perturbed state approach greatly reduced the numerical expense, however, significant expense was still required.

This work adapts and expands the perturbed state approach in two significant ways. The first (denoted as the direct approach in the text) is in a fundamental redefinition of the states of the system. By defining the states of the system to be concentration values rather than differential concentrations, the transition matrix is developed directly from the model, eliminating the need for state perturbations. This in turn reduces the numerical overhead while achieving very similar results to the perturbed state approach.

The second improvement is based on information from an error analysis of the projection. By understanding various components and sources of error in the projection, based on approximations inherent in the transition matrix, an error reduction strategy was developed and implemented. This approach periodically updated diffusion coefficient values and boundary diffusion coefficient and concentration values during projections based on the direct transition matrix approach. The numerical expense of updating can be significantly cheaper than running a full model due to the fact that the algebraic relationships of the Butler-Volmer equations do not have to be resolved. This approach, with the simplistic implementation presented here, has modest gains over the direct approach, however, greater improvements are undoubtedly achievable.

A case study was run to demonstrate the implementation of these projection approaches and significant reduction in numerical expense was seen. Although for the given loading conditions in the scenario presented, more simplistic base models of the battery could be used, the presented modeling approach can be used in a broader range of loading cases, has more direct correlation with physical parameters, and should be able to be adapted for even more extreme loading conditions than currently suited for. This approach can be used, for example, to explore design alternatives for loadings of this type. This will be of particular importance in regards to losses due to the parasitics in these systems. The parasitic capacitance of the battery could be a significant fraction of the losses in these loads that pulse the output battery voltage to extreme values, and may be a deciding factor as whether this loading of the battery is acceptable. Further work looking at the cause of these parasitics and the possible reduction will be important.

Other applications may be possible in that for the given loading condition and hardware used here, the simulation time was less than the computation time, suggesting that real time systems may be targeted. However, more extreme loadings may create a higher numerical cost and further adjustments and simplifications may need to be made for use in real time systems with those loadings. Additionally, this methods presented should be applicable to more complex battery dynamics and/or areas beyond the current electrochemical example.

Funding

This work was supported by the National Science Foundation [grant numbers NSF CMMI 0954422 and NSF CMMI 1435222].

References

[1] K.E. Thomas, J. Newman, R. Darling, Mathematical modeling of Lithium batteries, in: B. van Schalkwijk, B. Scrosati (Eds.), Advances in Lithium-ion Batteries, Kluwer Academic/Plenum Publishers, New York, NY, 2002 p. 362.
[2] S. Fabre, D. Guy-Bouyssou, P. Bouillon, F. Le Cras, C. Delacourt, Charge/discharge simulation of an all-solid-state thin-film battery using a one-dimensional model, J. Electrochem. Soc. 159 (2) (2012) A104–A115.
[3] D. Danilov, R. Niessen, P. Notten, Modeling all-solid-state Li-ion batteries, J. Electrochem. Soc. 158 (3) (2011) A215–A222.
[4] X. Hu, S. Li, H. Peng, A comparative study of equivalent circuit models for Li-ion batteries, J. Power Sources 198 (2012) 359–367.
[5] L. Gao, S. Liu, R. Dougal, Dynamic lithium-ion battery model for system simulation, IEEE Trans. Compon. Packag. Technol. 25 (3) (2002) 495–505.
[6] S. Santhanagopalan, Q. Guo, P. Ramadass, R. White, Review of models for predicting the cycling performance of lithium ion batteries, J. Power Sources 156 (2) (2006) 620–628.
[7] T. Kim, W. Qiao, A hybrid battery model capable of capturing dynamic circuit characteristics and nonlinear capacity effects, IEEE Trans. Energy Convers. 26 (4) (2011) 1172–1180.
[8] S. Afshar, Kirsten, A. Khajepour, Fully dynamical representation of a LFP battery cell, American Control Conference (ACC) (2017).
[9] L.M. Feeney, C. Rohner, P. Gunningberg, A. Lindgren, L. Andersson, How do the dynamics of battery discharge affect sensor lifetime? Wireless On-demand Network Systems and Services (WONS) (2014) 49–56.
[10] S. Park, A. Savvides, M. Srivastava, ACM, Battery capacity measurement and analysis using lithium coin cell battery, International Symposium on Lowpower Electronics and Design (ISLPED) (2001) 382–387.
[11] S. Castillo, et al., Experimental analysis of batteries under continuous and intermittent operations, International Conference on Embedded Systems and Applications (ESA) (2004) 18–24.
[12] K. Oldham, C. Rhee, J. Ryou, R. Polcawich, J. Pulskamp, Lateral thin-film piezoelectric actuators for bio-inspired micro-robotic locomotion, ASME International Design Engineering Technical Conferences (IDETC) (2009) 759–768.
[13] K. Teichert, K. Oldham, Dynamics and characteristics of thin film batteries cycled over capacitive load, IEEE International Conference on Advanced Intelligent Mechatronics (AIM), Banff, Canada, 2016.
[14] K. Teichert, K. Oldham, Modeling cyclic capacitive loading of thin-film batteries, J. Electrochem. Soc. 164 (2) (2017) A360–A369.

[15] C. Engstler, C. Lubich, Multirate extrapolation methods for differential equations with different time scales, Computing 58 (2) (1997) 173–185.
[16] E. Constantinescu, A. Sandu, Extrapolated multirate methods for differential equations with multiple time scales, J. Sci. Comput. 56 (1) (2013) 28–44.
[17] J. Roychowdhury, Analyzing circuits with widely separated time scales using numerical PDE methods, IEEE Trans. Circ. Syst. I—Fundam. Theory Appl. 48 (5) (2001) 578–594.
[18] D.A. Edwards, An alternative example of the method of multiple scales, SIAM Rev. 42 (2) (2000) 317–332.
[19] C. Kuehn, Multiple Time Scale Dynamics, Springer International Publishing, 2015.
[20] B. Hahn, Energy Efficient Iterative Adaptive On-Off Control of Capacitively-Loaded Actuators for Micro-robots, PhD, Mechanical Engineering, University of Michigan, 2012.
[21] J. Choi, et al., Thin-film piezoelectric and high-aspect ratio polymer leg mechanisms for millimeter-scale robotics, Int. J. Intell. Robot. Appl. 1 (2) (2017) 180–194.
[22] S.D. Fabre, D. Guy-Bouyssou, P. Bouillon, F. Le Cras, C. Delacourt, Charge/discharge simulation of an all-solid-state thin-film battery using a one-dimensional model, J. Electrochem. Soc. 159 (2) (2012) A104–A115, doi:http://dx.doi.org/10.1149/2.041202jes.
[23] M. Bowen, R. Smith, Derivative formulae and errors for non-uniformly spaced points, Proc. R. Soc. A—Math. Phys. Eng. Sci. 461 (2059) (2005) 1975–1997.
[24] R.L. Spencer, M. Ware, Computational Physics 430, Partial Differential Equations (Course Packet), Department of Physics and Astronomy, Brigham Young University, 2012.
[25] B. Edamana, B. Hahn, J.S. Pulskamp, R.G. Polcawich, K. Oldham, Modeling and optimal low-power on-off control of thin-film piezoelectric rotational actuators, IEEE/ASME Trans. Mechatron. 16 (5) (2011) 884–896.
[26] Cymbet Corporation, Enerchip CBC050, (2017) http://www.cymbet.com/pdfs/DS-72-01.pdf (Accessed 2017).